Mapping Pigmentation in Human Skin from a Multi-Channel Visible Spectrum Image by Inverse Optical Scattering Technique

Norimichi Tsumura,▲ Miki Kawabuchi, Hideaki Haneishi,▲ and Yoichi Miyake✦

Department of Information and Image Sciences, Chiba University, Chiba, Japan

Mapping pigmentation in human skin is expected to give useful information in reproducing skin color and enhancing the ability to diagnose various skin disease. In this research, maps of melanin, oxy-hemoglobin and deoxy-hemoglobin in skin are estimated from multi-channel visible spectrum image by using an inverse optical scattering technique. In the inverse optical scattering technique, first of all, a forward model of optical scattering is built to simulate the spectral reflectance of skin. Changing the variable parameters in the forward model, we repeat the simulation until the simulated spectral reflectance matches with the spectral reflectance at each pixel of the multi-spectral image. The principle of the proposed estimation technique was confirmed by imaging the human forearm under conditions of the venous occlusion, the venous and arterial occlusion, and by imaging a slapped region of the human forearm.

Journal of Imaging Science and Technology 45: 444–450 (2001)

Introduction

Extracting qualitative information and spatial distribution of components such as pigmentation through analyzing an observed image is required in many fields of image analysis such as remote sensing, medical diagnostics, and robot vision. Spectral characteristics of the components are useful information to identify the components, because different materials have different spectroscopic responses to electromagnetic waves of a certain energy band. A technique that uses a spectral image as an observed image was proposed[1] and has been expected to lead the field of image analysis.

Skin color reproduction may be considered the most important problem in color reproduction of color film and color television systems. With the recent progress of various imaging systems[2–4] such as multimedia, computer graphic and telemedicine systems, skin color becomes increasingly important for communication, image reproduction on hardcopy and softcopy, medical diagnosis, cosmetic development, etc. Human skin is a turbid medium with a multi-layered structure[5,6] and various pigments such as melanin and hemoglobin are contained in the medium. Slight changes in structure and pigmentation produce rich skin color variation. Therefore, it is necessary to analyze skin color on the basis of the structure and pigmentation in reproducing skin color and enhancing the ability to diagnose various skin disease.

Original manuscript received December 26, 2000

✦ IS&T Fellow

▲ IS&T Member

We have already proposed a technique to extract the map of skin pigmentation from skin color images[7] or skin spectral absorbance image[8] by independent component analysis. The facial color images were separated into the images that correspond to distribution of melanin and hemoglobin. The separated components were synthesized to simulate the various facial color images by changing the quantities of the two separated pigments. In the analysis of skin color, it was assumed that linearity among the quantities of pigment and the observed color signals holds in the optical density domain. However, the optical scattering in skin that causes the broad distribution of optical path length histogram in the skin may violate the linearity. It was also assumed that spectral absorbance of the pigment will not change spatially. However, hemoglobin has two states: oxy-hemoglobin (HbO_2), and deoxy-hemoglobin (Hb), and the ratio between HbO_2 and Hb will change spatially in a large area of skin image or in an area of skin diseases. The oxygen saturation is defined by the ratio between oxy-hemoglobin and total hemoglobin. Mapping oxygen saturation of blood in skin will give useful information for skin diagnosis.[9]

In this article, the pigmentations of melanin, oxy-hemoglobin and deoxy-hemoglobin in skin are estimated from a multi-channel visible spectrum image by using the inverse optical scattering technique. The reflected visible light will provide information only for the epidermis and dermis layers in the skin, because most of visible light does not penetrate into subcutis layer.

In the inverse optical scattering technique, first of all, a forward model of optical scattering is built to simulate the spectral reflectance of the skin. Changing the variable parameters in the forward model, the simulation is repeated until the simulated spectral reflectance matches with the spectral reflectance at each pixel of the multi-spectral image. The conventional non-linear

optimization technique is used to change the variable parameters at each iteration.

In the next section, oxygen saturation is briefly reviewed. This is an important diagnostic factor during and after operations, and the relation between oxygen saturation and skin color is described. Next, the forward model of optical scattering in human skin is described. The inverse optical scattering technique is explained based on the forward model. Finally, the experimental results of imaging the human forearm under venous occlusion, venous and arterial occlusion, and imaging a slapped region of the human forearm are shown.

Oxygen Saturation

The oxygen saturation So_2 is generally defined by the ratio between densities of oxy-hemoglobin and total hemoglobin as follows.

$$So_2 = [HbO_2] / ([Hb] + [HbO_2]) \quad (1)$$

where [Hb], [HbO_2] indicate the densities of deoxy-hemoglobin and oxy-hemoglobin respectively. The oxygen saturation of the arterial blood in a patient is usually monitored during and after the operation using a pulse oximeter, because hypoxia, the lack of oxygen in the body, is very dangerous during and after anesthesia in operations. The oxygen saturation level of 0.97 ~ 0.98 is normal in the arterial blood, about 0.70 is normal in venous blood.

The pulse oximeter analyzes the optical density toward transmitted near infrared light at the fingertip.[10] It is necessary to be concerned only with the attenuation of light by arterial blood in the total attenuation caused by arterial blood, venous blood, skin, muscle, bone, connective tissue, etc. It can be assumed that only the arterial blood changes its volume as the blood flows into and out of the vascular bed with pulsation. Therefore, it is possible to calculate the oxygen saturation of the arterial blood by subtracting the d.c. component of the attenuation from the total attenuation by the fingertip.

The near infrared light used in the pulse oximeter cannot be used to detect the pigmentation in skin layers because most of the near infrared light is transmitted by the skin. On the other hand, most visible light is diffusely reflected by the epidermis and dermis layers because skin layers have a strong scattering property for visible light. Therefore, the skin color is the light that is diffusely reflected by epidermis and dermis layers, along with absorption by pigments such as oxy-hemoglobin, deoxy-hemoglobin, and melanin. It will be effective to reproduce skin color based on the pigmentations considering the oxygen saturation that reflects the human physical and mental conditions. The oxygen saturation in skin layers is also expected to give useful information for diagnosing skin diseases such as psoriasis.[9] It is noted that pulsation can not be used in skin layers, and strong scattering also makes this measurement difficult without modeling the diffuse reflectance.

Forward Model of Optical Scattering in Skin

Monte Carlo Simulation for Light Transport in Multi-Layered Tissue

The earlier work of Wang and Jacques produced an excellent standard C-code for Monte Carlo simulation of light transport in multi-layered tissue (MCML).[11] Figure 1 is an example of how Wang and Jacques utilized such a simulation to model the propagation of a photon through a homogenous medium. Our research utilizes

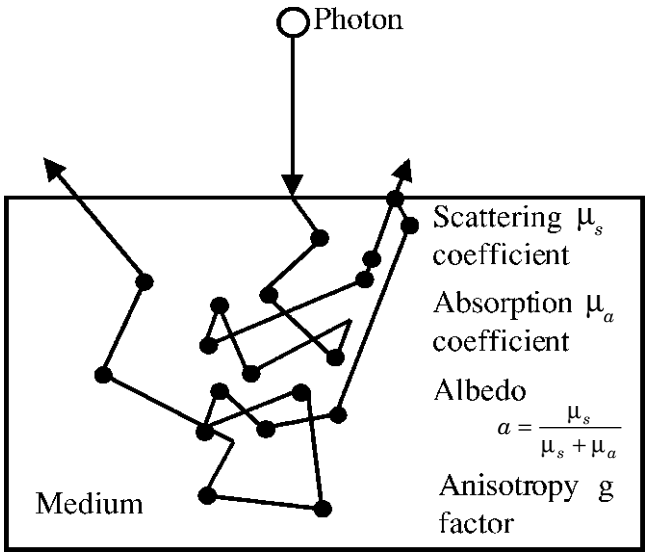

Figure 1. The movement of one photon through a homogenous medium, as calculated by Monte Carlo simulation.

the MCML program to simulate the spectral reflectance of skin.

The MCML program is constituted from following operations for photons.[12]

1. Photon launcing
2. Generating the propagation distance
3. Moving the photon
4. Internal reflection
5. Photon absorption
6. Changing photon direction by scattering
7. Calculating observable quantities

The Monte Carlo simulation begins by launching a photon into the tissue. Each propagation distance between photon positions is variable and equals $\Delta s = -\ln(\xi)/(\mu_a + \mu_s)$ where ξ is a random number and μ_a and μ_s are absorption and scattering coefficients, respectively. The photon's spatial position is described by three Cartesian coordinates. The direction of photon movement is described by three directional cosines. The directional cosines are denoted by μ_x, μ_y, and μ_z corresponding to the x, y, and z axes, respectively. The new coordinates (x', y', z') are calculated for a photon at (x, y, z) to the direction (μ_x, μ_y, μ_z) as follows.

$$\begin{aligned} x' &= x + \mu_x \Delta s \\ y' &= y + \mu_y \Delta s \\ z' &= z + \mu_z \Delta s \end{aligned} \quad (2)$$

The probability that the photon will be internally reflected is determined by the Fresnel reflection coefficient when the photon is propagated across a boundary into a region with a different index of refraction.

A weight is assigned to each photon to improve the efficiency of the Monte Calro program by assuming that many photons (a packet) propagate along the same pathway. The weight of the photon decreases with absorption from an initial value of 1 as it moves through the tissue, and equals a^n after n steps, where a is the albedo ($a = \mu_s/(\mu_a + \mu_s)$).

A normalized phase function describes the probability density function for the azimuthal and longitudinal

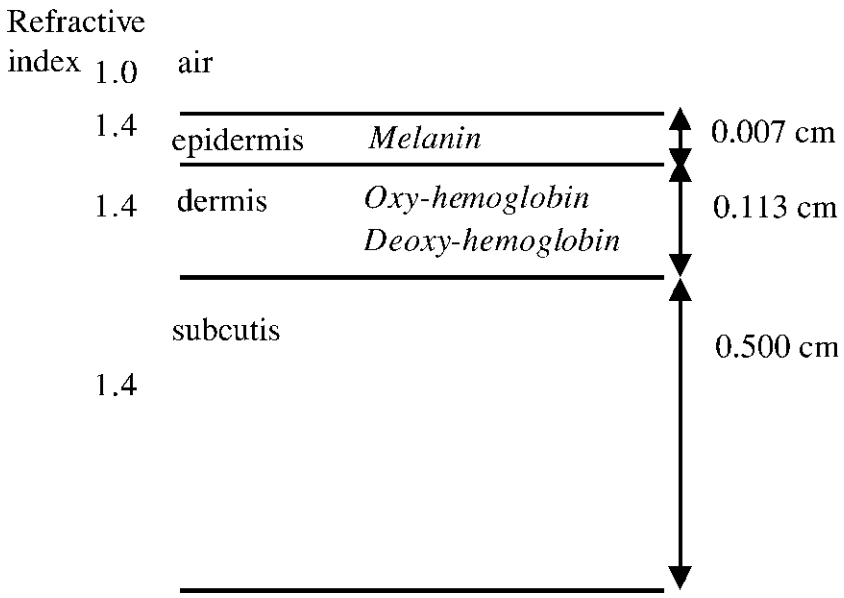

Figure 2. Three layered model of skin.

angles (θ, ϕ) for a photon when it is scattered. The scattering in tissue is easily characterized by the generating function for Henyey–Greenstein phase function as follows.

$$\cos\theta = \frac{1}{2g}\left\{1+g^2-\left[\frac{1-g^2}{1-g+2g\xi}\right]\right\} \tag{3}$$

where ξ is a uniformly distributed random number from 0 to 2π, the value of g is called the anisotropy factor of scattering. The various anisotropies characterize the type of scattering such as backward, forward, isotropic scatterings. If a photon is scattered at an angle (θ,ϕ) from the direction (μ_x, μ_y, μ_z) in which it is moving, then the new direction (μ'_x , μ'_y , μ'_z) is calculated by

$$\mu'_x = \frac{\sin\theta}{\sqrt{1-\mu_z^2}}\left(\mu_x\mu_z\cos\phi-\mu_y\sin\phi\right)+\mu_x\cos\theta$$

$$\mu'_y = \frac{\sin\theta}{\sqrt{1-\mu_z^2}}\left(\mu_y\mu_z\cos\phi-\mu_x\sin\phi\right)+\mu_y\cos\theta \tag{4}$$

$$\mu'_z = -\sin\theta\cos\phi\sqrt{1-\mu_z^2}+\mu_z\cos\theta$$

Many photon trajectories are calculated to yield a statistical description of photon distribution in the medium. The ratio between the sum of weights that escape from the surface and sum of initial weights used in the simulation gives the diffuse reflectance.

Three-Layered Model of Human Skin and its Spectral Reflectance by Monte Carlo Simulation

Figure 2 shows the three-layered model of skin, which is composed of the epidermis, dermis and subcutis layers. In this model, it is supposed that the skin color is dominated by the concentration of melanin in the epidermis layer, oxy-hemoglobin and deoxy-hemoglobin in the dermis layer. The refractive indices of air and tissue[13] are set to 1.0 and 1.4 respectively. The depths of epidermis, dermis and subcutis layers are set to 0.007 cm, 0.113 cm, and 0.5 cm respectively. The depth of epidermis layer was measured by ourselves for a male forearm. For this measurement, the technique of optical coherence tomography[14,15] was performed using the optical reflectometer (Hewlett-Packard Model HP 8504A). The depth of dermis layer is set to the measured mean value for a male forearm from Ref. 16. Ultrasonic diagnostic equipment was used for this measurement. The depth of subcutis layer is set empirically to reflect most of light into the dermis layer. The scattering coefficient and anisotropy factor used in epidermis and dermis layers are shown in Fig. 3, from Germert and co-workers.[17] The scattering coefficient and anisotropy factor in subcutis layer are set to 600 [cm^{-1}] and 0. 8 empirically at all wavelengths. The absorption cross sections of melanin, $\mu_a^{Melanin}$, oxy-hemoglobin μ^{aHbO2} and deoxy-hemoglobin μ_a^{Hb}, are shown in Fig. 4, from data of Anderson and coworkers.[6] In this research, variable parameters in the skin model are only the concentrations of melanin, $c^{Melanin}$, oxy-hemoglobin, c^{HbO2} and deoxy-hemoglobin, c^{Hb}.

Using the MCML program described above, diffuse reflectance in this three-layered skin model can be easily simulated. It is necessary to run the program for each wavelength to obtain the spectral reflectance using the spectral absorptions and scattering coefficients shown in Figs. 3 and 4. For single spectral reflectance of skin, therefore, we run the MCML programs 31 times, because the wavelength is sampled between 400 nm and 700 nm in the interval of 10 nm. One million photons were used for each wavelength in the program. To evaluate the error of the simulation, it was repeated 10 times changing the initial random value. Figure 5(a) shows the resultant averaged spectral reflectance for 10 simulations, where the concentrations of melanin, oxy-hemoglobin and deoxy-hemoglobin were set to 150, 9, and 1 [$x10^{-5}$ mol/L] respectively. The error, as standard deviation at each wavelength for 10 runs, is shown in Fig. 5(b). It is shown that the standard deviation of Monte Carlo simulation is under 3.5×10^{-4} in all wavelengths.

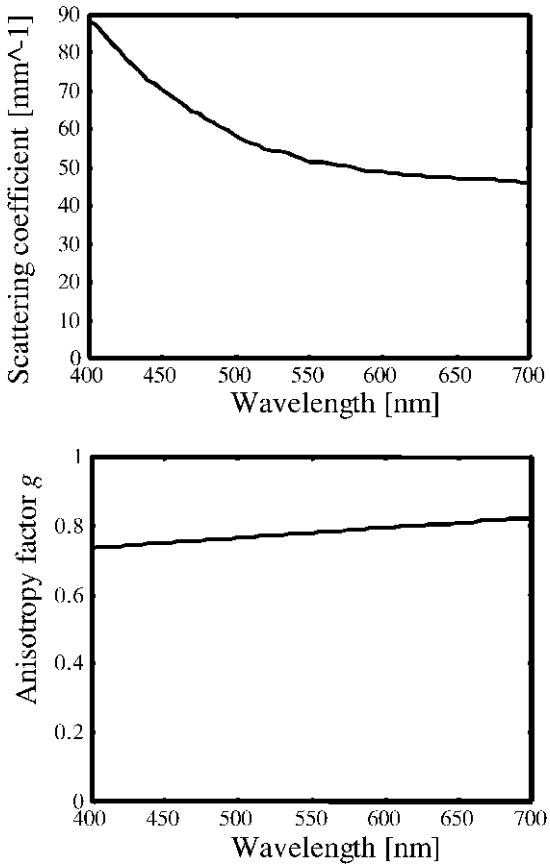

Figure 3. Scattering coefficient and anisotropy factor in epidermis and dermis layer.

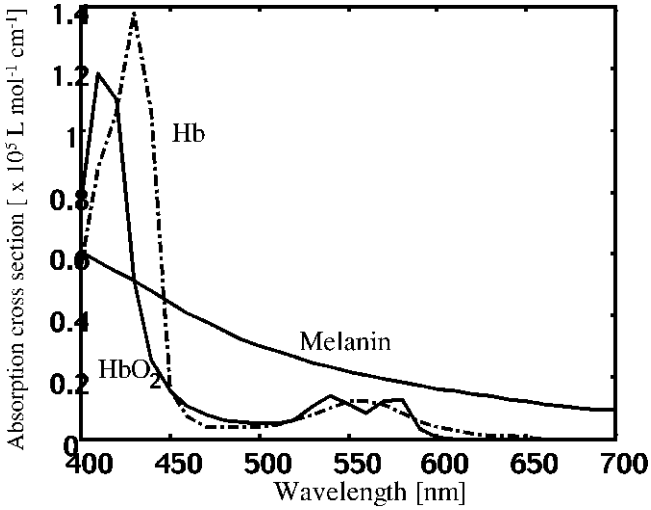

Figure 4. Absorption cross section of melanin, oxy-hemoglobin (HbO_2), and deoxy-hemoglobin (Hb).

Inverse Optical Scattering Technique

The concentration of pigments is estimated from diffuse spectral reflectance. Figure 6 shows the schematic diagram of the estimation method which involves successive approximations. At first, the initial values of variable parameters $c^{Melanin}, c^{HbO_2}, c^{Hb}$ are randomly given, and the spectral reflectance is simulated using the initial parameters based on the forward model of optical scattering in human skin. The amount of error between the simulated spectral reflectance and measured spectral reflectance is calculated. If the error is not small enough, the variable parameters are changed, and spectral reflectance is simulated again by using the changed parameters. If the error is small enough, the parameters used for the simulation become the results of the estimation. To determine change of parameters, a conventional optimization technique is used by MATLAB optimization tool box.[13] In this research, we used the reflectance at 580 nm, 610 nm and 640 nm for the estimation. Figure 7 shows examples of the estimation. In Fig. 7(a), concentrations of melanin and total hemoglobin are set for 150×10^{-5} mol/L, and 10×10^{-5} mol/L, respectively. The saturation is changed from 0.0 to 1.0. The horizontal axis indicates the target saturation value for the estimation, the vertical axis indicates the estimated saturation value by the above method. In Fig. 7(b), concentrations of total hemoglobin and saturation are set for 10×10^{-5} mol/L, and 0.9 respectively. The concentrations of melanin are changed from 0 to 300×10^{-5} mol/L. In Fig. 7(c), concentrations of melanin and saturation are set for 150×10^{-5} mol/L, and 0.9

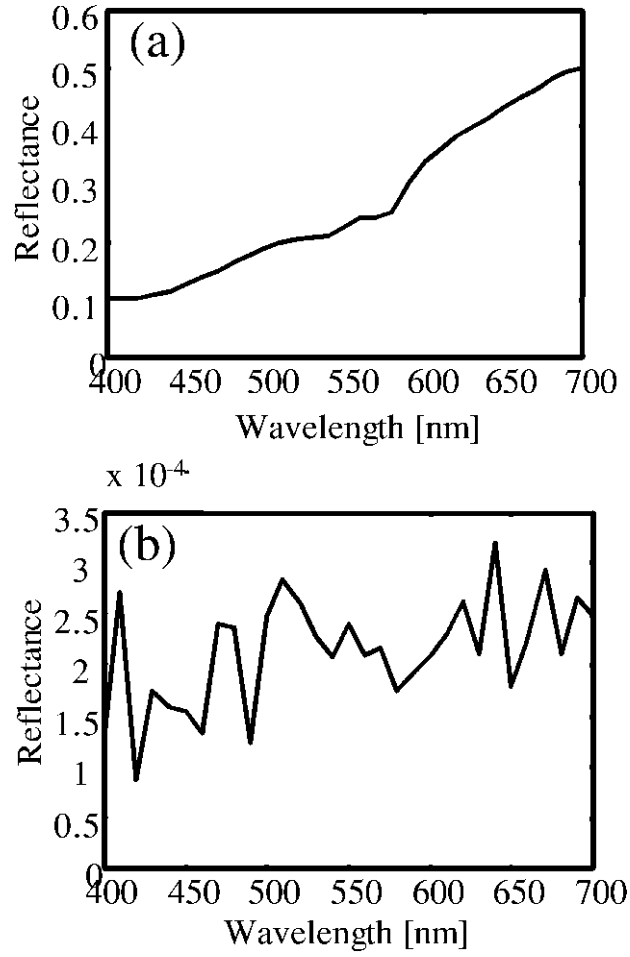

Figure 5. (a) Result of Monte Carlo simulation and (b) Standard deviation (error) in the simulation.

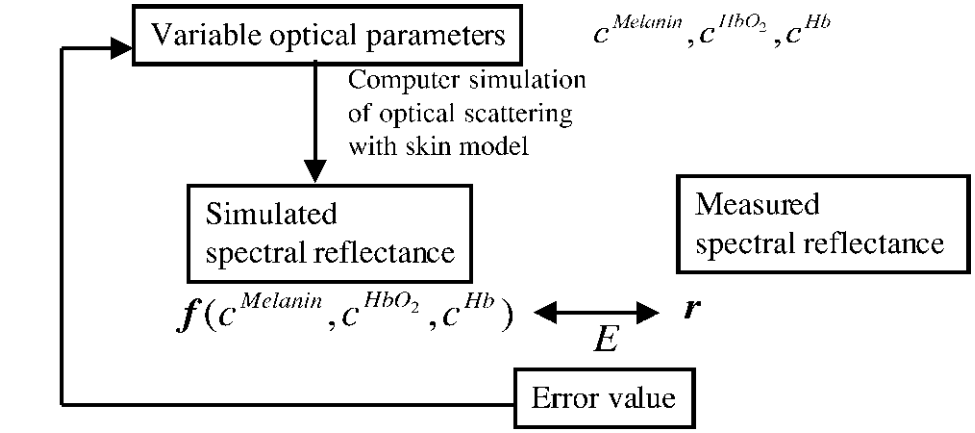

Figure 6. Estimation of concentrations of pigments from diffuse spectral reflectance.

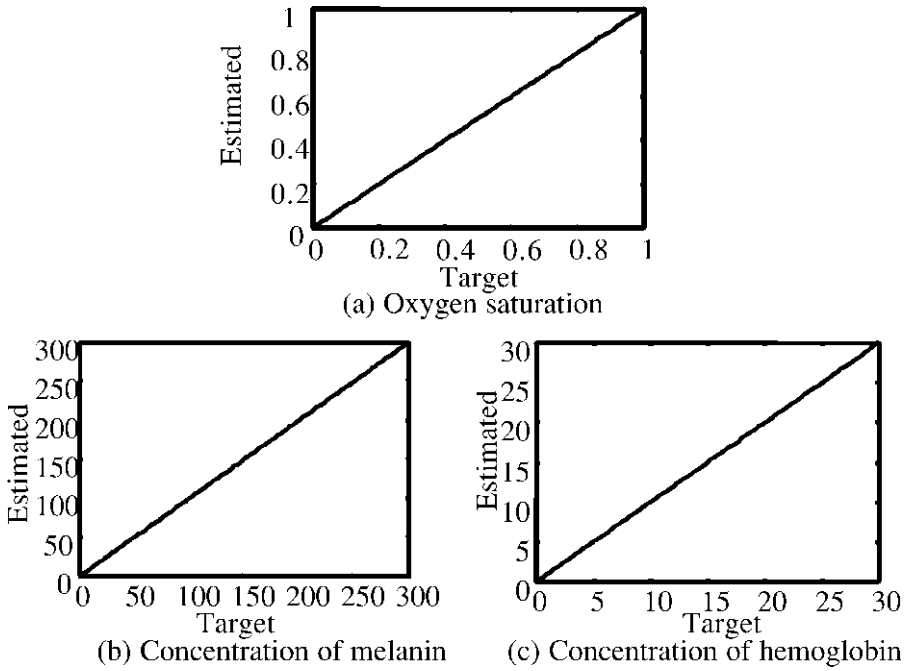

Figure 7. Results of estimation of concentrations of pigments from absolute diffuse spectral reflectance.

respectively. The concentrations of hemoglobin are changed from 0 to 30×10^{-5} mol/L. These results show that the concentrations and saturation are successfully estimated by the proposed technique.

Experiments

The imaging system consists of a standard white-light source (Natural Light NL–500, USHI/MURAKAMI) and a multi-spectral camera (OLYMPUS).[4] A wheel with 10 interference color filters is rotating between the lens and monochromatic CCD in the multi-spectral camera. The peak wavelengths of filter transmittance are arranged between 430 nm and 700 nm in 30 nm intervals. In our experiment, only three color filters, 580, 610, and 640 nm, were used for the estimation of pigmentation, because the images using other filters suffered strongly from noise strongly in the experiment. A reference white diffuse reflectance plate was placed on the skin and was used to calibrate the imaging system. During the occlusions in the elbow caused by a bandage, the skin image in the forearm of the subject was captured every 30 sec. The subject is a Japanese student in our laboratory. He was also the subject for measuring the depth of epidermis to model the skin structure. In the experiment, two types of occlusion, venous occlusion, arterial and venous occlusion, are performed as follows. The venous occlusion was achieved by applying a bandage softly to the elbow. On the other hand, combined arterial and venous

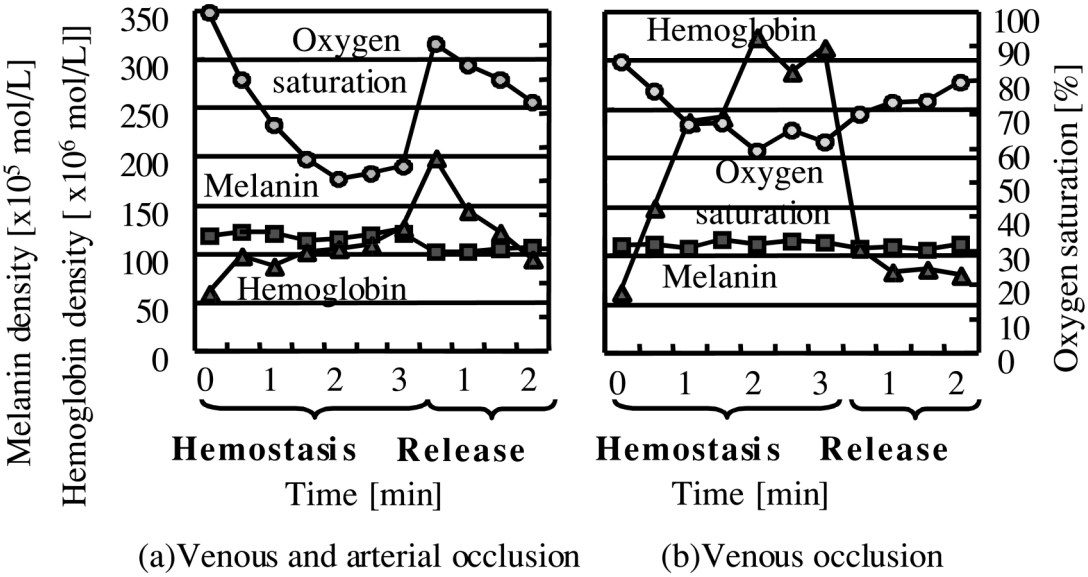

Figure 8. Results of estimation of concentrations of pigments from imaging the human forearm under (a) venous and arterial occlusion, (b) venous occlusion.

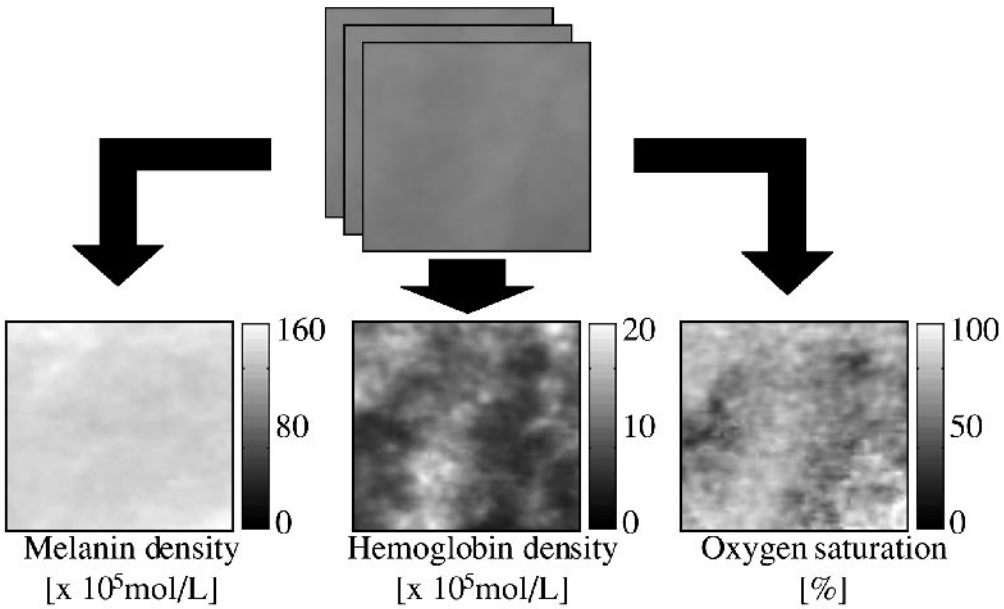

Figure 9. Results of estimation of concentrations of pigments from imaging the slapped region of the human skin.

occlusion was obtained by applying the bandage strongly. The strength of binding for both occlusions was adjusted empirically. The occlusions were continued for 3 min. After releasing the occlusions, the skin image was captured every 30 sec. Figure 8 shows the results of experiment. The oxygen saturation decreases more rapidly and decreases to a lower level for venous and arterial occlusion than for venous occlusion alone. On the other hand, the blood volume increases more rapidly and increases to a higher level for venous occlusion than for venous and arterial occlusion. The estimated concentration of melanin was almost constant during and after the occlusions. These results agree with physiological knowledge that concentration of melanin does not change on occlusions, but that concentration of hemoglobin will increase in congestion resulting from venous occlusion, and that oxygen saturation decrease with the change of inflow of arterial blood. Therefore, we think that the proposed technique is an effective means for estimating the 2-D distribution of the relative value of oxygen saturation, blood volume and pigmentation in the skin area. By imaging a slapped region of the human forearm, the increase of oxygen saturation and blood volume were imaged by our estimation technique as shown in Fig. 9.

Conclusion

The maps of melanin, oxy-hemoglobin and deoxy-hemoglobin in skin are estimated from multi-visible-spectral image by using the inverse optical scattering technique. Influences of noise, 3-D shape, specularity, skin types should be investigated in further studies. However, the results show the possibility to diagnose skin disease

from multi-channel visible spectrum imaging in collaboration with the medical community, and the resultant map will give useful information for reproducing various skin colors in spectral-based color management[3,4,18] and computer graphics.

Acknowledgment. The authors thank Mr. Tetsuya Tsugita and Mr. Koji Minami in Kao Corporation for supporting us in measuring the depth of epidermis by using their instrument.

References

1. S. Kawata, K. Sasaki and S. Minami, Component analysis of spatial and spectral patterns in multispectral images. I. Basis, *J. Opt. Soc. Amer. A* **4,** 2101–2106 (1987).
2. F. H. Imai, N. Tsumura, H. Haneishi, and Y. Miyake, Principal component analysis of skin color and its application to colorimetric color reproduction on CRT display and hardcopy, *J. Imaging Sci. Technol.* **40,** 422–430 (1996).
3. Y. Yokoyama, N. Tsumura, H. Haneishi, Y. Miyake, J. Hayashi, and M. Saito, A new color management system based on human perception and its application to recording and reproduction of art printing, in *Proc. of IS&T/SID's 5th Color Imaging Conference,* IS&T, Springfield, VA, 1997, pp. 169–172 .
4. M. Yamaguchi, R. Iwama, Y. Ohya, T. Obi, N. Ohyama, and Y. Komiya, Natural color reproduction in the television system for telemedicine, in Medical Imaging 1997: Image Display, Y. Kim, Ed., *Proc. SPIE* **3031,** 482–489 (1997).
5. M. J. C. van Gemert, S. L. Jacques, H. J. C. M. Sternborg, and W. M. Star, Skin optics, *IEEE Trans. on Biomedical Engineering* **36,** 1146–1154 (1989).
6. R. R. Anderson and J. A. Parrish, The optics in human skin, *J. Invest. Dermatology* **77,** 13–19 (1981).
7. N. Tsumura, H. Haneishi and Y. Miyake, Independent component analysis of skin color image, *J. Opt. Soc. Amer. A* **16,** 2169–2176 (1999).
8. N. Tsumura, H. Haneishi and Y. Miyake, Independent component analysis of skin absorbance image, *Opt. Rev.* **7**(6), 479–482 (2000).
9. P. J. Dwyer, R. R. Anderson and C. A. DiMarzio, Mapping blood oxygen saturation using a multi-spectral imaging system, in *Biomedical Sensing, Imaging, and Tracking Technologies II*, T. Vo-Dinh, R. A. Lieberman, and G. G. Vurek, Eds., *Proc. SPIE* **2976,** 270–280 (1997).
10. I. Yoshida, Y. Shimada and K. Tanaka, Spectrophotometric monitering of arterial oxygen saturation in the fingertip, *Med. Biol. Eng., Comput.* **18,** 27–32 (1980).
11. L. Wang and S. L. Jacues, Monte Carlo modeling of light transport in multi-layered tissues in Standard C, University of Texas M. D. Anderson Cancer Center (1992); http://omlc.ogi.edu/software/mc/index.html.
12. S. A. Prahl, M. Keijzer, S. L. Jacques, and A. J. Welch, A Monte Carlo model of light propagation in tissue, in *Dosimetry of Laser Radiation in Medicine and Biology*, G. Mueller and D. Sliney, Eds., *SPIE Series* **IS 5,** 102–111 (1989).
13. F. P. Bolin, L. E. Preuss, R. C. Taylor, and R. J. Ference, Refractive index of some mammalian tissues using a fiber optic cladding method, *Appl. Opt. Vol.* **28,** 2297–2303 (1989).
14. D. Huang, E. A. Swanson, C. P. Lin, J. S. Schuman, W. G. Stinson, W. Chang, M. R. Hee, T. Flotte, K. Gregory, C. A. Puliafito, and J. G. Fujimoto, Optical coherence tomography, *Science* **254,** 1178 (1991).
15. J. M. Schmitt, A. Knuttel, and R. F. Bonner, Measurement of optical properties of biological tissues by low-coherence reflectometry, *Appl. Opt.* **32,** 6032–6042 (1993).
16. M. Shimozuma, H. Nakagawa, F. Otsuka, and Y. Ishibashi, Application of ultrasonic diagnostic equipment in dermatology - measurement of skin thickness, *Japan. J. Dermatology*, **98,** 65–68 (1988). [in Japanese]
17. M. J. C. C. V. Gemert, S. L. Jacques, H. J. C. M. Sternborg, and W. M. Star, Skin optics, *IEEE Trans Biomed. Eng.* **36,** 1146 (1989).
18. M. R. Rosen, M. D. Fairchild, G. M. Johnson, and D. R. Wyble, Color Management within a Spectral Image Visualization Tool, in *Proceedings of IS&T/SID's 8th Color Imaging Conference*, IS&T, Springfield, VA, 2000, pp. 75–80.